Nanoscience and Nanometrology
2017; 3(1): 27-33
http://www.sciencepublishinggroup.com/j/nsnm
doi: 10.11648/j.nsnm.20170301.15
ISSN: 2472-3622 (Print); ISSN: 2472-3630 (Online)

Cr-Gd co-doped TiO_2 Nanoribbons as Photoanode in Making Dye Sensitized Solar Cell

Ghazi M. Abed[1], Abdulkareem M. A. Alsammarraie[2, *], Basim I. Al-Abdaly[2]

[1]Ministry of Science and Technology, Baghdad, Iraq
[2]Department of Chemistry, College of Science, University of Baghdad, Baghdad, Iraq

Email address:

karim.alsamuraee@gmail.com (A. M. A. Alsammarraie)
[*]Corresponding author

To cite this article:

Ghazi M. Abed, Abdulkareem M. A. Alsammarraie, Basim I. Al-Abdaly. Cr-Gd co-doped TiO_2 Nanoribbons as Photoanode in Making Dye Sensitized Solar Cell. *Nanoscience and Nanometrology*. Vol. 3, No. 1, 2017, pp. 27-33. doi: 10.11648/j.nsnm.20170301.15

Received: April 7, 2017; **Accepted**: April 26, 2017; **Published**: May 27, 2017

Abstract: Pure and (Cr^{3+}-Gd^{3+}) co-doped TiO_2 nanoribbons (TiNRs) were synthesized by a hydrothermal method at 200°C with stirring at 400 rpm. The structures and morphology of the prepared product were characterized using X-ray diffraction, Fourier transform infrared, Raman spectroscopy, Transmission electron microscopy and Scanning electron microscope. The results showed that the Cr^{3+} and Gd^{3+} metals ions dopant were incorporated into interstitial position of the TiO_2 lattice nanoribbons with diameter of (30-100) nm and length of few micrometers. The calculated optical band gap for undoped and co-doped of the TiNRs were 3.12 eV and 3.01, respectively. These modified properties of the TiNRs showed an important effect on the conversion efficiency of the assembled dye sensitized solar cells, where the efficiency of the undoped and co-doped TiNRs were 1.71 and 1.99, respectively.

Keywords: Doped TiO_2, DSSC, Nanoribbons

1. Introduction

Titanium dioxide (TiO_2) technologically is an important material owing to its notable chemical stability, combination of properties, and environment-friendly [1]. Therefore, great attention has paid to the research dealing with photocatalytic and catalytic properties in wide field of applications, ranging from the energy applications to environmental [2].

Nowadays, the researches show that the reaction between TiO_2 powder and concentrated NaOH solution under hydrothermal conditions is effective in forming one-dimensional 1-D structures of TiO_2 [3]. As nanostructures is a transition step bulk solid materials and crystal unit cells, these 1-D TiO_2-based structures, such as fibers, nanotubes, and ribbons, have an important interests, where it could exhibit novel physicochemical properties and reaction behaviors [4].

The doping of transition metals (TMs) in the TIO_2 help in forming new energy levels between conduction band (CB) bottom and valence band (VB), involving a shift of light absorption towards the region of the visible light. Usually, the activity of Photocatalytic is based on the nature and the amount of doping elements [5]. The doping of TiO_2 with rare-earth elements (REEs) has attracted significant attention regarding its unique 4f electronic configuration, catalytic properties and special luminescent. Multiple electronic configurations can be easily generated and the oxide is polymorphism exhibiting strong adsorption selectivity and good thermal stability. Especially, after doping there is remarkable shift to the visible range [6].

A solar cell directly converts solar energy into electrical power using a semiconductor. Recently, dye-sensitized solar cells (DSSCs) have considered as an attractive alternative for third solar cells generation due to their convenient of manufacturing, high efficiency of power conversion and low cost. Comparing with other organic cells, the dye-sensitized solar cells (DSSCs) is an effective method owing to their high conversion efficiency. The DSSCs consist of five main components transparent conducting glass, semiconductor materials, dyes as a sensitizer, redox-couple electrolyte and counter electrode [7].

In this study the undoped TiO_2 and Cr/Gd co-doped TiO_2 nanoribbons via hydrothermal method have prepared from

TiO_2 nanoparticles. In addition, the effect of Cr/Gd dopant on the fabrication and characterization of the dye sensitized solar cell (DSSCs) has been evaluated.

2. Experimental

2.1. Synthesis TiO_2 Nanoparticles (TiNPs)

TiNPs were synthesized by sol–gel [8] utilizing titanium (IV) isopropoxide (TTIP), distilled water, ethyl alcohol, and HCl as the starting materials. Concentrations the volume ratio of [TTIP: EtOH: H_2O: HCl] were chosen as (1:7:0.35:0.07). (7 ml) of TTIP was dissolved in 30 ml of anhydrous ethanol to prepare solution A. Meanwhile, 0.5 ml of concentrated HCl was mixed with 20 ml of anhydrous ethanol and 2.5 ml of water to prepare solution B. Solution A was subsequently added dropwise to solution B under vigorous stirring within 30 min. A homogeneous solution was obtained after stirring vigorously for 2h, and a sol was formed. After 24h, the sol was transformed into gel and in order to obtain nanoparticals and the product was separated by centrifugations. Then the product has dried at 80°C for 12h. The dried gel was annealed at 400°C for 4h, to acquire the desired TiO_2 NPs.

2.2. Synthesis of Undoped TiO_2 Nanoribbons (TiNRs)

The details of the synthesis steps for the TiNRs were reported in hydrothermal method [9]. Briefly, 0.5 g of Titanium(IV) oxide was mixed with 50 ml of 10 M NaOH alkaline solution and the suspension system had stirred for 1h at RT. Then, the resultant mixture had moved into a teflon-lined autoclave, at 200°C and constant magnetic stirring at 400 rpm for 72h. The obtained precipitates from centrifuging process had washed with deionized water. Afterward, the products underwent an ultrasonic treatment with 0.1 M HCl and then washed by distilled water equal to pH=7 of washing solution was obtained. Finally, the product powder of TiNRs was placed into a ceramic crucible for annealing at 400°C for 4h.

2.3. Synthesis of Cr-Gd co-doped TiNPs

[Cr^{3+}-Gd^{3+}] co-doped TiNRs were prepared as follows: The synthesized anatase TiO_2 powder nanoparticles, (0.5 g), was stirred with (50 ml) of 10 mol/l NaOH aqueous solution containing 0.5 mol% each of Chromium(III) nitrate nonahydrate $Cr(NO_3)_3.9H_2O$ and Gadolinium(III) nitrate hexahydrate $Gd(NO_3)_3.6H_2O$ for 1 h at room temperature to form a suspension. Afterward, the mixed solution was transferred into a Teflon-lined autoclave. The final precipitate was treated in the same manner to obtain the TiNRs.

2.4. Fabrication of Photoelectrodes and DSSCs

The FTO glass was used as substrate after careful cleaning. Fabrication of photo anodes using TiO_2 NPs and TiNRs which mixed at ratios (100% TiNPs, 75% TiNPs: 25% TiNRs) with total weight of 1 g and ground in a mortar. Ethanol (20 ml), deionized water (2 ml), and CH_3COOH (0.5 ml) were added dropwise to diffuse the TiO_2 NPs and TiNRs under ultrasonic probe. The TiO_2 composite moved with an excess of ethanol (50 ml) into beaker and stirred at 300 rpm for 3h. Then the composite had concentrated by evaporating. The paste was coated on FTO coated glass by tape casting method. Then the films that had formed were sintered at 450°C for 15 min and at 500°C for 15 min in air. After cooling to 80°C, the TiO_2 electrodes were immersed into (0.5 mM) N3-535 dye solution and kept at room temperature for (20–24 h) to insure complete sensitizer uptake. The platinum-coated FTO is used as the counter. A drop of electrolyte solution was injected into the photoelectrode and then the counter was clamped onto the photoelectrode; the electrolyte solution prepared by dissolving (0.5M) of KI and (0.05M) of I^- in ethylene glycol. Solar cell assembly; the cell assembly was performed by adding a few drops of (I^-/ I_3^-) electrolyte on the photoanode and fix both electrodes (anode and counter) electrodes facing each other using a clips binder. Finally all the assembled DSSCs are tested by two electrodes potentiostat using (100mW/cm^2) deuterium light source.

3. Results and Discussion

3.1. Scanning Electron Microscopic (SEM)

The SEM micrographs, morphology and particles size distribution of the precursor TiO_2 nanoparticles obtained by sol-gel methods (Figure 1). The morphology of the sample refers to uniform nanostructures with average size 30-50 nm.

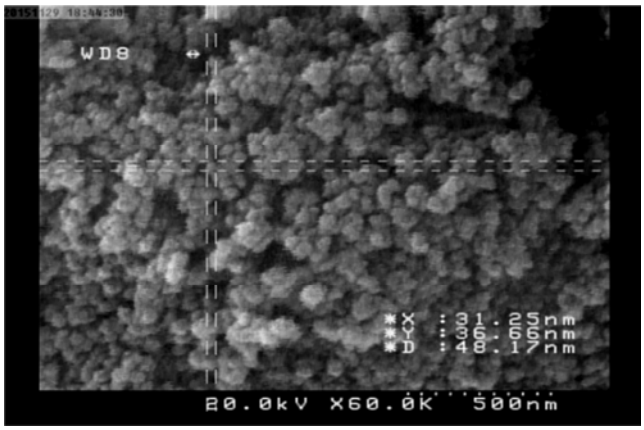

Figure 1. *SEM images of TiO_2 nanoparticles.*

The SEM micrographs results of undoped TiO_2 and [(Cr^{3+}-Gd^{3+}) co-doped TiNRs prepared by hydrothermal method at 200°C for 72 h followed by heat treatment at 400°C for 3h are shown in Figure 2 (a and b).

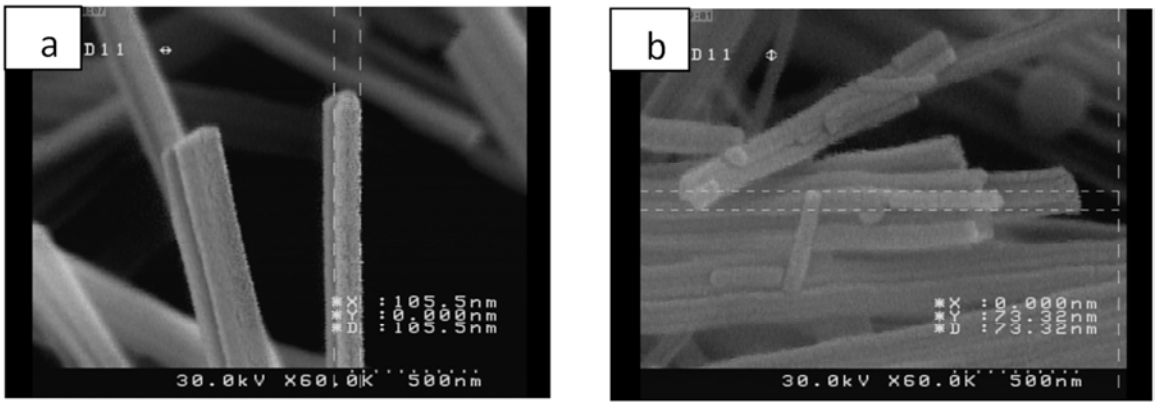

Figure 2. *SEM images of (a) undoped TiNRs (b) [Cr^{3+}-Gd^{3+}] co-doped TiNRs.*

The images show the presence long and straight of ribbon-like with typical lengths is ranging from several micrometers to tens of micrometers. These samples are confirmed the well-defined 1D TiNRs without any sign of an impurity cluster.

3.2. Transmission Electron Microscopy (TEM)

Figure 3 (a and b), is a low-magnification TEM images of undoped TiNRs and (Cr^{3+}-Gd^{3+}) co-doped TiNRs, as-grown samples, showing the ribbon-like structure. The width of the ribbons varies from 30 to 250 nm, and the geometry of the ribbons are quite uniform.

In contrast, These surface morphologies of TiNRs are not affected by the Chromium and Gadolinium doping, indicating that (Cr^{3+}-Gd^{3+}) are successfully incorporated into the TiO_2 lattice crystal, thus eliminating any impurity and confirming that (Cr^{3+}-Gd^{3+}) metal clusters are forming from the morphological point of view.

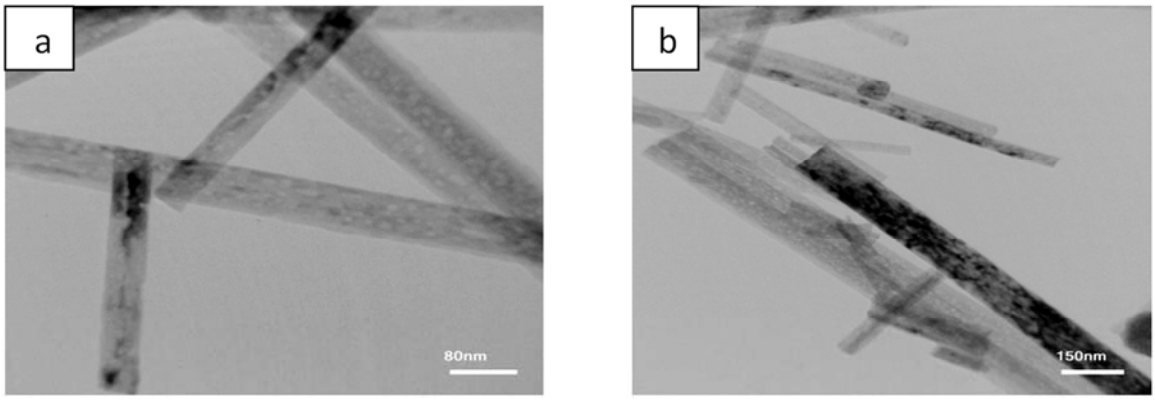

Figure 3. *TEM images of (a) undoped TiNRs, (b) [$Cr^{3+}Gd^{3+}$] co-doped TiNRs.*

In hydrothermal reaction, TiNRs were obtained during the reaction of high concentration of NaOH aqueous solution and pure TiO_2 powder in Teflon line stainless autoclave at suitable hydrothermal temperature and time. The reaction is defined by sequence reaction step below:

a) High concentrated alkaline reaction

At the first reaction step, the high concentrated of NaOH (alkaline solution) will reacted with TiO_2 powder at temperature of 200°C for 72h. The sodium titanate ($Na_2Ti_2O_5.H_2O$) was the main product.

$$2TiO_2 + 2NaOH \rightarrow Na_2Ti_2O_5.H_2O \quad (1)$$

b) Replacement of Na+ with H+

The hydrogenotitanate was formed during the ion exchange between Na^+ and H^+ occurs during the acid wash treatment. The reason for this sodium titanate was thermodynamically unstable. The general chemical reaction can be described as follows:

$$N_aTi_2O_5.H_2O + xH^+ \rightarrow H_xNa_{2-x}Ti_2O_5.H_2O + xNa^+, (0 \leq x \leq 2) \quad (2)$$

c) Dehydration process

The dehydration process is performed by undergone drying process at 80°C overnight and followed by calcination process at high temperature for two hours. The reaction consists of two steps as follows:

$$H_2Ti_2O_5.H_2O \rightarrow H_2Ti_2O_5 + H_2O \quad (3)$$

$$H_2Ti_2O_5 \rightarrow 2TiO_2 + H_2O \quad (4)$$

3.3. X-ray Diffraction and ICP

X-ray diffraction (XRD) pattern of starting TiO_2 nanoparticles (TiNPs) prepared by sol gel method is shown in Figure 4 (a). The peaks observed at 2θ = 25.35°, 37.62°, 48.20°, 53.68°, 55.25°, and 62.91° correspond to the

reflection planes (101), (004), (200), (105), (211) and (204) respectively, which confirms the formation of well crystallized pure anatase TiO_2 phase with minor rutile titania phase at $2\theta = 27.52°$. All peaks are in good agreement with the standard spectrum (JCPDS no. 84-1286)[10].

The XRD results of the hydrothermally prepared undoped TiO_2 and (Cr^{3+}-Gd^{3+}) co-doped TiO_2 using 10 M NaOH and constant magnetic stirring at 400 rpm at 200°C for 72 h are shown in Figure 4 (b and c). XRD patterns illustrate that all of prepared materials are a mixed phase combination of both TiO_2 anatase and TiO_2-(B). It can be seen that two XRD peak positions of anatase phase are detected at around $2\theta = 24.12°$ and 48.20° which corresponds to (101) and (200) planes respectively. Near these two peaks there are another two peaks corresponding (110) and (020) peaks of TiO_2-(B). The XRD pattern shows different peaks of TiO_2-(B) at $2\theta = 14.11°$, 28.58° and 43.30° which correspond to the reflection planes (200), (002), (003) respectively. These results are in agreement with the (JCPDS no. 46-1238, monoclinic [11]. Rutar et al. (2015) showed that the transformation from TiO_2-(B) to anatase was completed at 650°C [2]. The result was a mix of two phases (anatase and TiO_2-(B)) because we have used in our calcination process 400°C. Police et al (2010) confirmed that no peaks of dopant were observed in XRD pattern due to low concentration of dopant loading into TiNRs [12]. The XRD cannot identify the dopant peaks because of their detection limit.

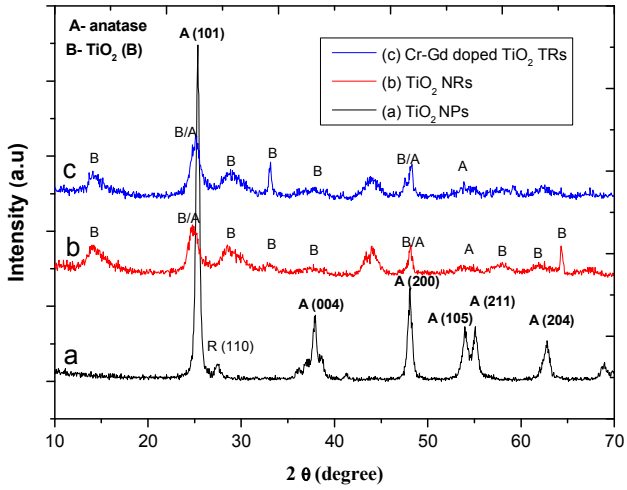

Figure 4. *XRD patterns of (a) TiO_2 NPs, (b) undoped TiNRs, (c) (Cr^{3+}-Gd^{3+}) co-doped TiNRs.*

The result of (Cr^{3+}-Gd^{3+}) in the doped TiO_2 NRs measured by the Inductively Coupled Plasma-Optical Emission spectroscopy (ICP-OES). Greene et al. (2006) confirms the doping process is complex in aqueous system because the doping species would form metal-aquo complexes easily and not incorporate into the crystal lattice [13]. The final doping level is approximately (0.43 and 0.39)% which is lower than the (Cr/Gd) concentration in the precursor solution. The difference between the theoretical and the measured concentration of (Cr/Gd) in the $Ti_{1-x}M_xO_2$ samples is due to the incomplete degree of hydrothermal reaction of substrates during the synthesis of $Ti_{1-x}M_xO_2$. The colored solution after hydrothermal treatment at washing process, confirms that not all the (Cr/Gd) in solution was consumed during the hydrothermal synthesis.

3.4. Raman Spectroscopy

Raman spectra were used for further characterization of the anatase TiO_2 nanoparticles, undoped TiO_2 NRs, and [(Cr^{3+}-Gd^{3+})] co-doped TiO_2 NTs (Figure 5). The Raman peaks observed at 142, 197, 391, 514 and 634 cm^{-1} in Figure 5 (a) are assigned as the E_g-1, E_g-2, B_{1g}, B_{1g}+A_{1g}, and E_g-3 modes of anatase phase, respectively. The peak located at 634 cm^{-1} (E_g-3) for Ti−O stretching mode, the peak at 514 cm^{-1} (B_{1g}+A_{1g}) refer to Ti−O stretching mode, and the peak appeared at 391 cm^{-1} (E_g-2) assigned to the O−Ti−O bending mode [14].

In our case study the peaks at 141, 179, 284, 376, 461, 482 and 656 cm^{-1} observed for the undoped TiO_2 nanoribbons (Figure 5 (b and c)), synthesized at 200°C /72h and peaks at 153, 195, 300, 467, 489, and 677 cm^{-1} observed for the [(Cr^{3+}-Gd^{3+})] co-doped titanate nanoribbons. The peaks are almost consistent with both obtained spectra of undoped and co-doped. Peaks at (141, 153) cm^{-1} are corresponding to Eg phonon mode of anatase [15]. The peak at (179, 195) cm^{-1} assigned to Na−O−Ti modes [16]. The peak at (284, 300) cm^{-1} is correspond to Ti−O bonds in sodium titanate at the range of bands (656-677) cm^{-1} of the undoped and the [(Cr^{3+}-Gd^{3+})] co-doped TiNRs were assigned to a Ti−O−Ti vibration [17].

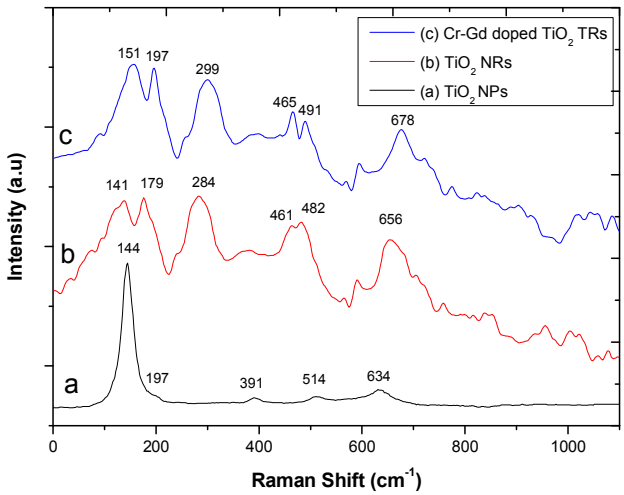

Figure 5. *Raman spectra of (a) TiO_2 NPs, (b) undoped TiNRs, (c) (Cr^{3+}-Gd^{3+}) co-doped TiNRs.*

3.5. Fourier Transform Infrared Spectroscopy

The studied samples were characterized by FT-IR analysis in the range between (4000-400) cm^{-1}, where the FT-IR results for the TiNPs are shown in Figure 6 (a), and undoped/doped TiNRs are shown in Figure 6 (b and c). The results show the existence of hydroxyl groups in all samples. The broad peak at 3300-3500 cm^{-1} is referred to the stretching vibrations of O−H group, which is attributed to the significant amount of H_2O

molecules in the interlayer space and surface. The peak at 1630-1640 cm^{-1} could belong to the bending vibration of H−O−H group on the all nanostructures [18]. The peak at about 486 cm^{-1} might be a sign to bending modes of TiO_6 [19, 20]. The broad band (from about 800 till 400 cm^{-1}) was assigned to Ti−O and Ti−O−Ti skeletal frequency region. The sodium ions present in the samples are not only physically adsorbed but also incorporate within the lattice, and the composition is other than titanium dioxide [21].

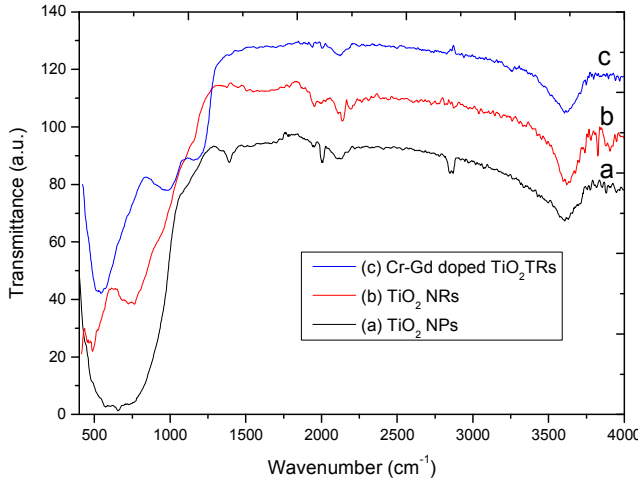

Figure 6. *FTIR spectrum of (a) TiO_2 NPs, (b) undoped TiNRs, (c) (Cr^{3+}-Gd^{3+}) co-doped TiNRs.*

3.6. UV-Visible Spectroscopy

The optical absorbance coefficient of a semiconductor close to the band edge can be expressed by the following equation:

$$\alpha = \frac{A(h_v - E_g)n}{h_v} \quad (5)$$

Where a α is the absorption coefficient, E_g is the absorption band gap, A is constant, n depends on the nature of the transitions and may have values (½, 2, $^3/_2$ and 3) depending on the allowed direct, allowed indirect, forbidden direct and forbidden indirect transitions respectively [22]. The absorption spectra of TiO_2 nanoparticles are shown in Figure 7A (a). The absorption band edges were estimated to be about 381 nm.

The band gap energy can be determined by extrapolation to the zero coefficients, which is calculated from the above equation. As shown in Figure 7B, the intercept of the tangent to the plot $(\alpha h\upsilon)^2$ versus hυ gives a good estimation of the band gap for this semiconductor of direct band gap. The band gap value of 3.21 eV is for sol-gel derived TiO_2 nanoparticles. Light absorption characteristics of the hydrothermally synthesized 1D TiO_2 NRs and the precursor TiO_2 are shown in Figure 7A (a) (b). The as-synthesized sample exhibit a red shift of the absorption edge and considerable absorption in the visible violet region. As a result of doping process, the band gap is slightly decreased (Figure 7 (c)). According to the TiO_2 energy band structure, the CB bottom and VB top correspond mainly to O 2p and Ti 3d states, respectively [23]. The optical absorption around 378 nm for undoped TiO_2 is only due to the band-to-band (O 2p → Ti 3d) transition, while the slight red shift in [(Cr^{3+}-Gd^{3+})] co-doped TiO_2 NRs can be explained as being mainly due to (sp-d) exchange interactions between the band electrons and the localized (d-f) electrons of the ions substituting cations. The s-(d-f) and p-(d-f) exchange interactions give rise to downward shifting of the CB edge and an upward shifting of the VB edge, causing a band gap narrowing [24]. The indirect band gap was determined by the linear fit to the linear portion of the $(\alpha h\upsilon)^2$ versus photon energy (hυ) plot (Figure 7B (b), (c)). The calculated band gap of undoped, and 1 mol% [(Cr^{3+}-Gd^{3+})] co-doped TiNRs are (3.12, 3.01) eV, respectively.

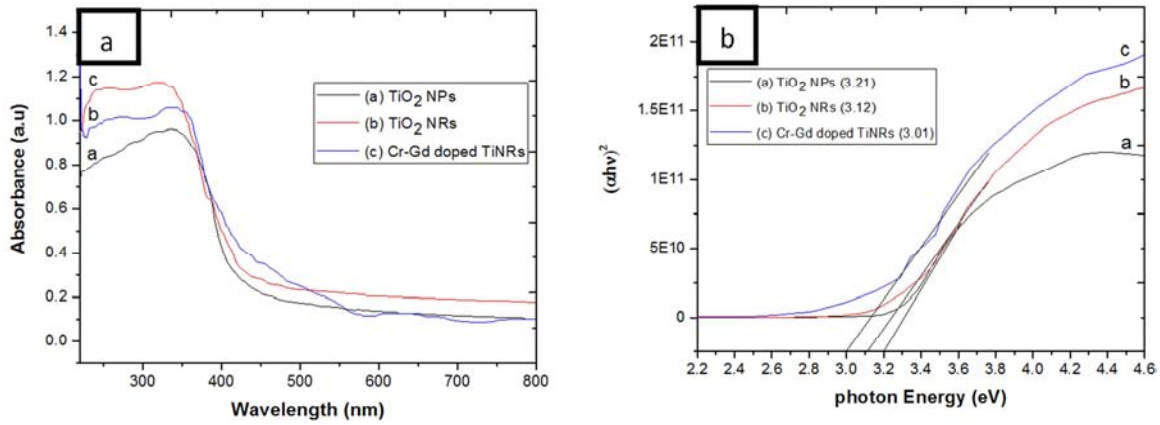

Figure 7. *(A) UV-visible absorption spectra of (a) TiO_2 nanoparticles, (b) undoped TiNRs, (c) [Cr^{3+}-Gd^{3+}] co-doped TiNRs, (B) $(\alpha h\upsilon)^2$ vs. photon energy for (a) TiO_2 nanoparticles, (b) undoped TiNRs, (c) [Cr^{3+}-Gd^{3+}] co-doped TiNRs.*

3.7. DSSCs Based on Composite TiO_2 NPs/TNRs

Figure 8 shows the current-voltage photovoltaic performance curves of DSSCs based on the (a); pure TiO_2-NPs cell, (b); (75:25) wt.% TiO_2-NPs/TiO_2 TiNRs, (c); (75:25) wt.% TiO_2-NPs/[Cr^{3+}-Gd^{3+}] co-doped TiNRs cells, under AM 1.5 illumination (100 mW/cm^2). The energy conversion efficiencies (η%) and the full factors are

calculated using equations (6) and (7) respectively and are listed in Table 1.

$$ff = \frac{I_{max} * V_{max}}{I_{sc} * V_{oc}} \quad (6)$$

$$\% \eta = \frac{I_{sc} * V_{oc}}{Pinput} * ff * 100 \quad (7)$$

Table 1. *Calculated energy conversion (η%) and full factor (FF) of DSSC using hybrid TiO_2 NPs/TiNRs.*

No.	photoanodes	V_{oc} (mV)	I_{sc} (mA/cm^2)	Vmax (mV)	Imax (mA/cm^2)	η(%)	FF
a	TiO_2-NPs	544	6.49	426	4.81	2.04	0.58
b	TiO_2-NPs/TiO_2-TNRs	503	5.73	402	4.27	1.71	0.59
c	TiO_2-NPs/(Cr^{3+}-Gd^{3+})doped- TNRs	530	6.82	392	5.10	1.99	0.55

The best energy conversion efficiency 2.04 with full factor of 0.58 was achieved with using TiO_2-NPs. The co-doping with these two metals are applied to further increase energy conversion efficiency, where each element can separately enhance device properties [25]. In addition, one element can reinforce the effect of the other [26], or may counteract some of the detrimental effects caused by the other element [27]. Cr^{3+} doping of TiO_2 led to a clear red shift in the UV/Vis absorption spectrum, evidencing a decrease in band gap and VB shift, which resulted in a slightly lower value of V_{oc} [28], while the worst was on using TiO_2-NPs/TiO_2-TNRs, where η% was at minimum 1.71 and the FF was 0.59. This can be attributed to less surface area which reduces the adsorption of the dye [29], and consequently the TiNRs collected electron number is reduced.

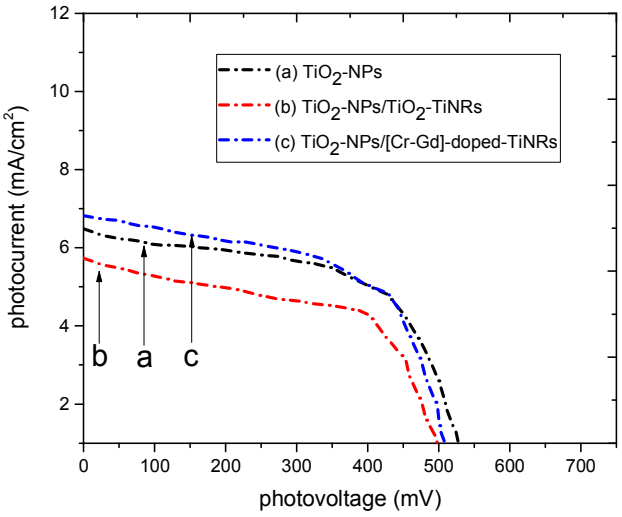

Figure 8. *I-V characteristic of DSSC using hybrid TiO_2 NPs/TiNRs.*

4. Conclusions

The aim of this study is to synthesize the undoped and co-doped TiO_2 nanoribbons from the TiO_2 nanoparticles prepared by sol gel method using alkaline hydrothermal method. Both TiO_2 nanoribbons and TiO_2 nanoparticles are used as photoanode in making the dye sensitized solar cell. Then we evaluate the effect of doping process of TiO_2 nanoribbons on the DSSCs efficiency. Shape and size of the TiNRs could be controlled by the reaction temperature and the reaction time. Yet, it is long time method with complicated alkaline washing process. The conversion efficiency of the co-doping TiNRs is better than undoped TiNRs, while the conversion efficiency of TiO_2 NPs of DSSC was the best.

References

[1] Chen, X. and Mao, S. S., 2007. Titanium dioxide nanomaterials: synthesis, properties, modifications, and applications, Chem. Rev, vol. 107, no. 7, pp. 2891–2959.

[2] Rutar, M., Rozman, N., Pregelj, M., Bittencourt, C., Korošec, R. C., Škapin, A. S., Mrzel, A., Škapin, S. D. and Umek, P., 2015. Transformation of hydrogen titanate nanoribbons to TiO_2 nanoribbons and the influence of the transformation strategies on the photocatalytic performance, Beilstein J. Nanotechnol., vol. 6, no. 1, pp. 831–844.

[3] Jin Z. L. and Lu, G.-X., 2005. Efficient Photocatalytic Hydrogen Evolution over Pt x-/TiO_2-y B y Catalysts in a Ternary System of K+, Mg^{2+}/$B_4O_7^{2-}$/H_2O," Energy & fuels, vol. 19, no. 3, pp. 1126–1132.

[4] Zhu, H., Zheng, Z., Gao, X., Huang, Y., Yan, Z., Zou, J., Yin, H., Zou, Q., Kable, S. H., Zhao, J. and others, 2006. Structural Evolution in a Hydrothermal Reaction between Nb_2O_5 and NaOH Solution: From Nb_2O_5 Grains to Microporous $Na_2Nb_2O_6.2/3H_2O$ Fibers and $NaNbO_3$ Cubes, J. Am. Chem. Soc., vol. 128, no. 7, pp. 2373–2384.

[5] Demeestere, K., Dewulf, J., Ohno, T., Salgado, P. H. and H. Langenhove, V., 2005. Visible light mediated photocatalytic degradation of gaseous trichloroethylene and dimethyl sulfide on modified titanium dioxide, Appl. Catal. B Environ., vol. 61, no. 1, pp. 140–149.

[6] Xie, Y., and Yuan, C., 2004. Rare earth ion modified TiO_2 sols for photocatalysis application under visible light excitation, RARE Met. Ed., vol. 23, no. 1, pp. 20–26.

[7] Regan, O., Gratzel, M., (1991) A low-cost, high-efficiency solar cell based on dye-sensitized colloidal TiO_2 films. Nature 353:737–739).

[8] Nadzirah, S., Foo, K. L. and Hashim, U., 2015. Morphological reaction on the different stabilizers of titanium dioxide nanoparticles. Int J Electrochem Sci, 10, pp. 5498-5512.

[9] Sekino, T., 2010. Synthesis and applications of titanium oxide nanotubes. In Inorganic and Metallic Nanotubular Materials (pp. 17-32). Springer Berlin Heidelberg.

[10] Zeng, Y. Z., Liu, Y. C., Lu, Y. F. and Chung, J. C., 2014. Study on the Preparation of Nanosized Titanium Dioxide with Tubular Structure by Hydrothermal Method and Their Photocatalytic Activity. International Journal of Chemical Engineering and Applications, 5 (3), p. 234.

[11] Chimupala, Y., Hyett, G., Simpson, R. and Brydson, R., 2014. Synthesis and characterization of a mixed phase of anatase TiO_2 and TiO_2 (B) by low pressure chemical vapour deposition (LPCVD) for high photocatalytic activity. In Journal of Physics: Conference Series (Vol. 522, No. 1, p. 012074). IOP Publishing.

[12] Police, A. K. R., Pulagurla, V. L. R., Vutukuri, M. S., Basavaraju, S., Valluri Durga, K. and Machiraju, S., 2010. Photocatalytic degradation of isoproturon pesticide on C, N and S doped TiO_2. Journal of Water Resource and Protection, 2010.

[13] Greene, L. E., Yuhas, B. D., Law, M., Zitoun, D. and Yang, P., 2006. Solution-grown zinc oxide nanowires. Inorganic chemistry, 45 (19), pp. 7535-7543.

[14] Mikami, M., Nakamura, S., Kitao, O. and Arakawa, H., 2002. Lattice dynamics and dielectric properties of TiO_2 anatase: a first-principles study. Physical Review B, 66 (15), p. 155213.

[15] Ribbens, S., Meynen, V., Van Tendeloo, G., Ke, X., Mertens, M., Maes, B. U. W., Cool, P. and Vansant, E. F., 2008. Development of photocatalytic efficient Ti-based nanotubes and nanoribbons by conventional and microwave assisted synthesis strategies. Microporous and Mesoporous Materials, 114 (1), pp. 401-409.

[16] Choi, H. C., Jung, Y. M. and Kim, S. B., 2004. Characterization of Raman spectra of size-selected TiO_2 nanoparticles by two-dimensional correlation spectroscopy. Bulletin of the Korean Chemical Society, 25 (3), pp. 426-428.

[17] Hardcastle, F. D., 2011. Raman spectroscopy of titania (TiO_2) nanotubular water-splitting catalysts. Journal of the Arkansas Academy of Science, 65 (1), pp. 43-48.

[18] Sauvet, A. L., Baliteau, S., Lopez, C. and Fabry, P., 2004. Synthesis and characterization of sodium titanates $Na_2Ti_3O_7$ and $Na_2Ti_6O_{13}$. Journal of Solid State Chemistry, 177 (12), pp. 4508-4515.

[19] Viana, B. C., Ferreira, O. P., Souza Filho, A. G., Hidalgo, A. A., Mendes Filho, J. and Alves, O. L., 2011. Highlighting the mechanisms of the titanate nanotubes to titanate nanoribbons transformation. Journal of Nanoparticle Research, 13 (8), pp. 3259-3265.

[20] Peng, H., Lai, K., Kong, D., Meister, S., Chen, Y., Qi, X. L., Zhang, S. C., Shen, Z. X. and Cui, Y., 2010. Aharonov-Bohm interference in topological insulator nanoribbons. Nature materials, 9 (3), pp. 225-229.

[21] Qamar, M., Yoon, C. R., Oh, H. J., Lee, N. H., Park, K., Kim, D. H., Lee, K. S., Lee, W. J. and Kim, S. J., 2008. Preparation and photocatalytic activity of nanotubes obtained from titanium dioxide. Catalysis Today, 131 (1), pp. 3-14.

[22] Zhao, Y., Li, C., Liu, X., Gu, F., Jiang, H., Shao, W., Zhang, L. and He, Y., 2007. Synthesis and optical properties of TiO_2 nanoparticles. Materials Letters, 61 (1), pp. 79-83.

[23] Santara, B., Giri, P. K., Imakita, K. and Fujii, M., 2013. Evidence of oxygen vacancy induced room temperature ferromagnetism in solvothermally synthesized undoped TiO_2 nanoribbons. Nanoscale, 5 (12), pp. 5476-5488.

[24] Loan, T. T. and Long, N. N., 2016. Optical Properties of Anatase and Rutile TiO_2: Cr^{3+} Powders. VNU Journal of Science: Mathematics-Physics, 30 (2).

[25] Ko, K. H., Lee, Y. C. and Jung, Y. J., 2005. Enhanced efficiency of dye-sensitized TiO_2 solar cells (DSSC) by doping of metal ions. Journal of colloid and interface science, 283 (2), pp. 482-487.

[26] Zhang, J. C., Han, Z. Y., Li, Q. Y., Yang, X. Y., Yu, Y. and Cao, W. L., 2011. N, S-doped TiO_2 anode effect on performance of dye-sensitized solar cells. Journal of Physics and Chemistry of Solids, 72 (11), pp. 1239-1244.

[27] Berglund, S. P., Hoang, S., Minter, R. L., Fullon, R. R. and Mullins, C. B., 2013. Investigation of 35 Elements as Single Metal Oxides, Mixed Metal Oxides, or Dopants for Titanium Dioxide for Dye-Sensitized Solar Cells. The Journal of Physical Chemistry C, 117 (48), pp. 25248-25258.

[28] Xie, Y., Huang, N., You, S., Liu, Y., Sebo, B., Liang, L., Fang, X., Liu, W., Guo, S. and Zhao, X. Z., 2013. Improved performance of dye-sensitized solar cells by trace amount Cr-doped TiO_2 photoelectrodes. Journal of Power Sources, 224, pp. 168-173.

[29] Lamberti, A., Sacco, A., Bianco, S., Manfredi, D., Cappelluti, F., Hernandez, S., Quaglio, M. and Pirri, C. F., 2013. Charge transport improvement employing TiO_2 nanotube arrays as front-side illuminated dye-sensitized solar cell photoanodes. Physical Chemistry Chemical Physics, 15 (7), pp. 2596-2602.